epl A Letters Journal Exploring the Frontiers of Physics

January 2009

EPL, **85** (2009) 29001 www.epljournal.org
doi: 10.1209/0295-5075/85/29001

Tachyonic γ-ray cascades from BL Lacertae objects

R. Tomaschitz[(a)]

Department of Physics, Hiroshima University - 1-3-1 Kagami-yama, Higashi-Hiroshima 739-8526, Japan

received 28 November 2008; accepted in final form 15 December 2008
published online 28 January 2009

PACS 98.54.Cm – Active and peculiar galaxies and related systems (including BL Lacertae objects, blazars, Seyfert galaxies, Markarian galaxies, and active galactic nuclei)
PACS 52.27.Ny – Relativistic plasmas
PACS 95.30.Gv – Radiation mechanisms; polarization

Abstract – Evidence for superluminal radiation from TeV blazars is pointed out. Spectral fits of the BL Lacertae objects W Comae, 1ES 2344 + 514, PG 1553 + 113, and 1ES 0806 + 524 are performed with tachyonic γ-ray cascades generated by the thermal electron plasma in the galactic nuclei. The transversal and longitudinal radiation components as well as the thermodynamic parameters of the ultra-relativistic electron populations are extracted from the spectral maps based on EGRET, VERITAS, MAGIC, and HESS flux data. An extended spectral plateau typical for tachyonic γ-ray spectra emerges in the MeV and low GeV range, terminating in exponential decay without a power law crossover. Thermal tachyonic cascade spectra are also predicted for Fermi blazars. By comparing to other TeV γ-ray sources such as Galactic supernova remnants and pulsar wind nebulae as well as active galactic nuclei, the curvature in the high-energy spectral slopes of BL Lacertae objects is shown to be intrinsic, *i.e.* uncorrelated with distance.

Introduction: Tachyonic spectral densities of ultra-relativistic electrons. – We perform a tachyonic cascade fit to a GeV γ-ray flare of the active galactic nucleus W Comae [1,2], as well as to γ-ray spectra of the TeV blazars 1ES 2344 + 514 [3], PG 1553 + 113 [4], and 1ES 0806 + 524 [5]. In contrast to GeV–TeV photons, the extragalactic tachyon flux is not attenuated by interaction with the cosmic background light. There is no absorption of tachyonic γ-rays via pair creation, as tachyons do not interact with infrared background photons. We show that the curvature in the γ-ray spectra of BL Lacertae objects (BL Lacs) is caused by the Boltzmann factor of the ultra-relativistic electron plasma in the galactic nucleus rather than by intergalactic absorption, in accordance with the tachyonic radiation model.

The quantized tachyonic radiation densities of uniformly moving electrons read [6,7]

$$p^{\mathrm{T,L}}(\omega,\gamma) = \frac{\alpha_{\mathrm{q}} m_{\mathrm{t}}^2 \omega}{\omega^2+m_{\mathrm{t}}^2}\left[\gamma^2 - \frac{m_{\mathrm{t}}}{m}\frac{\omega}{m_{\mathrm{t}}}\gamma - \frac{1}{4}\frac{m_{\mathrm{t}}^2}{m^2} - \left(1+\frac{\omega^2}{m_{\mathrm{t}}^2}\right)\Delta^{\mathrm{T,L}}\right]\frac{1}{\gamma\sqrt{\gamma^2-1}}, \quad (1)$$

where the superscripts T and L refer to the transversal/longitudinal polarization components defined by $\Delta^{\mathrm{T}} = 1 - m_{\mathrm{t}}^2/(2m^2)$ and $\Delta^{\mathrm{L}} = 0$. m and γ denote the electron mass and the electronic Lorentz factor, $m_{\mathrm{t}} \approx 2.15\,\mathrm{keV}$ is the tachyon mass, and $\alpha_{\mathrm{q}} \approx 1.0\times 10^{-13}$ the tachyonic fine-structure constant estimated from hydrogenic Lamb shifts [8]. A spectral cutoff occurs at

$$\omega_{\max} = m_{\mathrm{t}}\left(\mu_{\mathrm{t}}\sqrt{\gamma^2-1} - \frac{1}{2}\frac{m_{\mathrm{t}}}{m}\gamma\right), \qquad \mu_{\mathrm{t}} = \sqrt{1+\frac{1}{4}\frac{m_{\mathrm{t}}^2}{m^2}}. \quad (2)$$

Only frequencies in the range $0 \leqslant \omega \leqslant \omega_{\max}(\gamma)$ can be radiated by a uniformly moving charge [6], and a positive $\omega_{\max}(\gamma)$ requires Lorentz factors exceeding the threshold μ_{t} in (2).

Spectral averaging over thermal electron populations. – We average the radiation densities (1) with a thermal ultra-relativistic Maxwell-Boltzmann distribution,

$$\mathrm{d}\rho(\gamma) = A\mathrm{e}^{-\beta\gamma}\sqrt{\gamma^2-1}\gamma\mathrm{d}\gamma. \quad (3)$$

The electron number is found via $n_1 = \int_{\mu_{\mathrm{t}}}^{\infty}\mathrm{d}\rho(\gamma)$, which defines the normalization factor A. The exponential cutoff is related to the electron temperature by $\beta = m/(kT)$.

(a) E-mail: tom@geminga.org

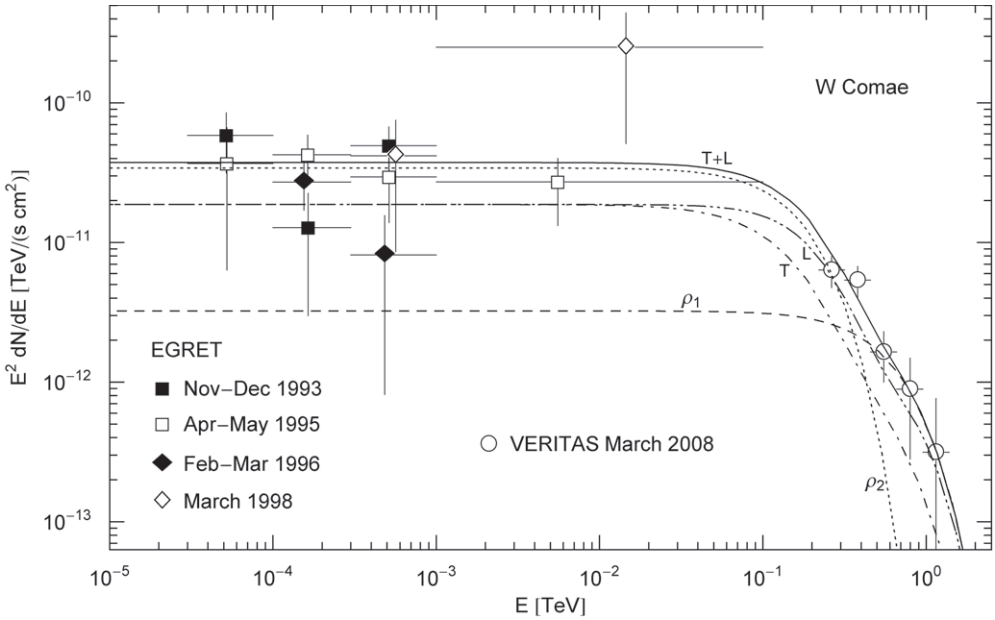

Fig. 1: γ-ray wideband of the BL Lac object W Comae. VERITAS flux points from ref. [9], EGRET points refer to the associated source 3EG J1222 + 2841, cf. ref. [11]. The solid line T + L depicts the unpolarized differential tachyon flux $\mathrm{d}N^{\mathrm{T+L}}/\mathrm{d}E$, obtained by adding the flux densities $\rho_{1,2}$ of two ultra-relativistic electron populations, cf. table 1. The transversal and longitudinal flux densities $\mathrm{d}N^{\mathrm{T,L}}/\mathrm{d}E$ add up to the total unpolarized flux T + L, cf. (7). The EGRET flux points define a spectral plateau in the MeV to GeV range typical for tachyonic cascade spectra [6,13,19].

The average is carried out as

$$\langle p^{\mathrm{T,L}}(\omega)\rangle = \int_{\mu_{\mathrm{t}}}^{\infty} p^{\mathrm{T,L}}(\omega,\gamma)\theta(\omega_{\max}(\gamma)-\omega)\mathrm{d}\rho(\gamma), \qquad (4)$$

where θ is the Heaviside step function. The spectral range of the radiation densities (1) is bounded by $\omega_{\max}$ in (2), so that the solution of $\omega = \omega_{\max}(\hat{\gamma})$ defines the minimal electronic Lorentz factor for radiation at this frequency,

$$\hat{\gamma}(\omega) = \mu_{\mathrm{t}}\sqrt{1+\omega^2/m_{\mathrm{t}}^2} + \frac{1}{2}\frac{\omega}{m}. \qquad (5)$$

The average (4) can be reduced to

$$\begin{aligned} \langle p^{\mathrm{T,L}}(\omega)\rangle &= B^{\mathrm{T,L}}(\omega,\hat{\gamma}(\omega)),\\ B^{\mathrm{T,L}}(\omega,\gamma_1) &= \textstyle\int_{\gamma_1}^{\infty} p^{\mathrm{T,L}}(\omega,\gamma)\mathrm{d}\rho(\gamma), \end{aligned} \qquad (6)$$

with the density $\mathrm{d}\rho(\gamma)$ given in (3) and the Lorentz factor $\hat{\gamma}(\omega)$ in (5). The superscripts T and L denote the transversal and longitudinal radiation components. The spectral fits in figs. 1–5 are based on the E^2-rescaled differential flux densities

$$E^2\frac{\mathrm{d}N^{\mathrm{T,L}}}{\mathrm{d}E} = \frac{\omega}{4\pi d^2}\langle p^{\mathrm{T,L}}(\omega)\rangle, \qquad (7)$$

where d is the distance to the source and $\omega = E/\hbar$. The rescaling with E^2 is useful, as it reveals the curvature of rapidly decaying spectral slopes.

Tachyonic cascade fits of TeV blazars. – In fig. 1, a γ-ray flare of W Comae (W Com, ON 231) observed with the imaging atmospheric Cherenkov telescope VERITAS in March 2008 [9] is studied in association with the unidentified EGRET source 3EG J1222 + 2841 [10]. The MeV to GeV flux points of the γ-ray wideband in fig. 1 were recorded with the EGRET instrument on board the Compton Gamma Ray Observatory during four viewing periods in 1993-1998 [11]. The spectral fit is shown in figs. 1 and 2; the tachyonic cascades ρ_i are plots of the rescaled flux densities (7). The fit is performed with the unpolarized flux $\mathrm{d}N^{\mathrm{T+L}}/\mathrm{d}E = \mathrm{d}N^{\mathrm{T}}/\mathrm{d}E + \mathrm{d}N^{\mathrm{L}}/\mathrm{d}E$ generated by thermal electron populations ρ_i, cf. (3) and table 1. Each electron density generates a cascade ρ_i, and the wideband comprises two cascade spectra.

The spectral plateau in fig. 1 (extending over the MeV range to low GeV energies) and the curved spectral slope defined by the VERITAS points in fig. 2 are reproduced by the cascade fit. As for the electronic source number, cf. after (3), we use a rescaled parameter $\hat{n}$ for the fit,

$$\hat{n} = \frac{\alpha_{\mathrm{q}} n_1}{\hbar\,[\mathrm{keV\,s}]\,4\pi d^2\,[\mathrm{cm}]} \approx 1.27\times 10^{-45}\frac{n_1}{d^2\,[\mathrm{Mpc}]}, \qquad (8)$$

which is independent of the distance estimate in (7). Here, $\hbar\,[\mathrm{keV\,s}]$ implies the tachyon mass in keV units in the spectral functions $B^{\mathrm{T,L}}$ in (6). At γ-ray energies, only a tiny $\alpha_{\mathrm{q}}/\alpha_{\mathrm{e}}$ fraction (the ratio of tachyonic and electric fine-structure constants) of the tachyon flux is absorbed by the detector, which requires a rescaling of the electron number n_1, so that the actual number of radiating electrons is $n^{\mathrm{e}} = n_1\alpha_{\mathrm{e}}/\alpha_{\mathrm{q}} \approx 7.3\times 10^{10} n_1$, cf. ref. [12]. We

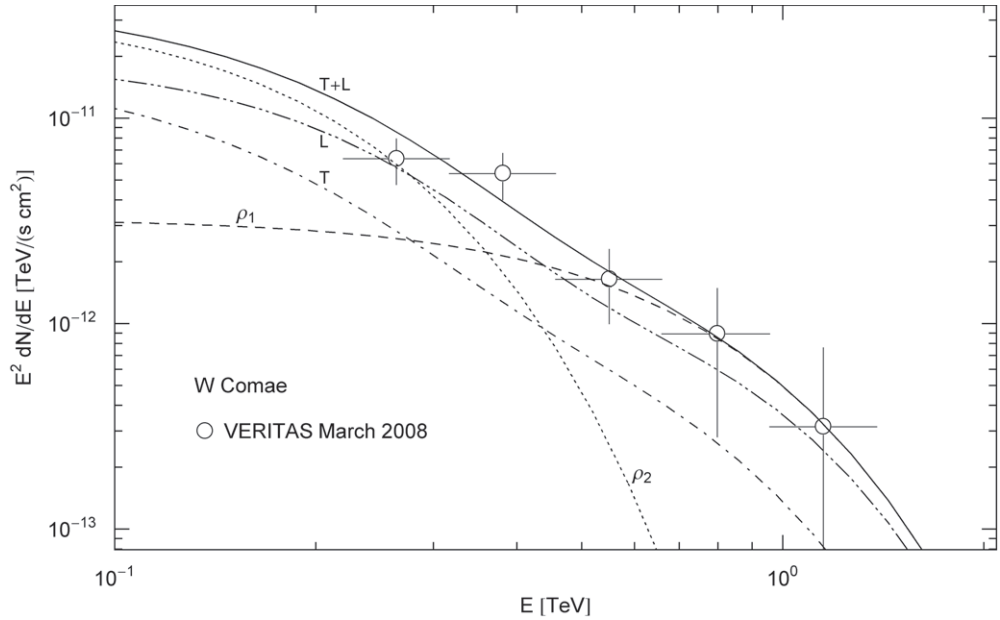

Fig. 2: Close-up of the VERITAS flare spectrum in fig. 1. T and L stand for the transversal and longitudinal flux components, and $\mathrm{T}+\mathrm{L}=\rho_1+\rho_2$ labels the unpolarized flux. The exponential decay of the cascades $\rho_{1,2}$ sets in at about $E_{\mathrm{cut}}\approx(m_{\mathrm{t}}/m)\,kT$, where $m_{\mathrm{t}}/m\approx 1/238$ is the tachyon-electron mass ratio [8], implying cutoff energies of 240 GeV for the ρ_1 cascade and 67 GeV for ρ_2.

Table 1: Electronic source distributions ρ_i generating the tachyonic γ-ray spectra of the BL Lac objects in figs. 1–5. $\rho_{1,2}$ denote thermal ultra-relativistic Maxwell-Boltzmann densities (3) with cutoff parameter β in the Boltzmann factor. $\hat{n}$ determines the amplitude of the tachyon flux generated by the electron density ρ_i. The electron count n^{e} is calculated at the indicated distance d estimated from the quoted redshift, cf. after (8). kT is the temperature and U the internal energy of the thermal electron populations ρ_i, cf. (9). The distance estimates do not affect the spectral maps but the electron number n^{e}. Regarding blazar PG $1553+113$, the electron count and internal energy are listed for two different redshift estimates [4,16]. The tachyonic γ-ray cascades labeled $\rho_{1,2}$ in the figures are produced by the corresponding electronic source distributions in this table. Each cascade depends on two fitting parameters β and $\hat{n}$, cf. (3) and (8), extracted from the χ^2 fit $\mathrm{T}+\mathrm{L}$ in the figures.

	β	$\hat{n}$	d (Mpc)	n^{e}	kT (TeV)	U (10^{60} TeV)
W Comae						
ρ_1	8.78×10^{-9}	3.5×10^{-4}	$z\approx0.102$	4.1×10^{57}	58.2	0.71
ρ_2	3.16×10^{-8}	3.7×10^{-3}	450	4.3×10^{58}	16.2	2.1
1ES $2344+514$						
ρ_1	7.68×10^{-10}	7.1×10^{-5}	$z\approx0.044$	1.5×10^{56}	665	0.30
ρ_2	9.77×10^{-9}	8.6×10^{-4}	190	1.85×10^{57}	52.3	0.29
PG $1553+113$						
ρ_1	2.15×10^{-9}	7.0×10^{-5}	$z\approx0.36$	1.0×10^{58}	238	7.1
ρ_2	3.31×10^{-8}	4.4×10^{-3}	1600	6.5×10^{59}	15.4	30
ρ_1	2.15×10^{-9}	7.0×10^{-5}	$z\approx0.1$	7.8×10^{56}	238	0.56
ρ_2	3.31×10^{-8}	4.4×10^{-3}	440	4.9×10^{58}	15.4	2.3
1ES $0806+524$			$z\approx0.138$			
ρ_1	1.33×10^{-8}	3.0×10^{-4}	610	6.4×10^{57}	38.4	0.74

thus find the electron count as $n^{\mathrm{e}}\approx5.75\times10^{55}\hat{n}d^2$ [Mpc], where $\hat{n}$ determines the tachyonic flux amplitude extracted from the χ^2 fit. The redshift $z\approx0.102$ of W Com translates into a distance of 450 Mpc via $d\,[\mathrm{Mpc}]\approx4.4\times10^3 z$, that is $d\sim cz/H_0$, with $h_0\approx0.68$.

The cutoff energy of the thermal cascades depends on the electron temperature $kT\,[\mathrm{TeV}]\approx5.11\times10^{-7}/\beta$, cf. the caption of fig. 2. The energy estimates of the electronic source populations in table 1 are based on $U\,[\mathrm{TeV}]\sim1.53\times10^{-6}n^{\mathrm{e}}/\beta$, which is the high-temperature limit of the internal energy of a relativistic Fermi gas,

$$U=3\frac{mn^{\mathrm{e}}}{\beta}\left(1+\frac{\pi^2}{32}\frac{\beta^3n^{\mathrm{e}}}{m^3V}+\dots\right). \tag{9}$$

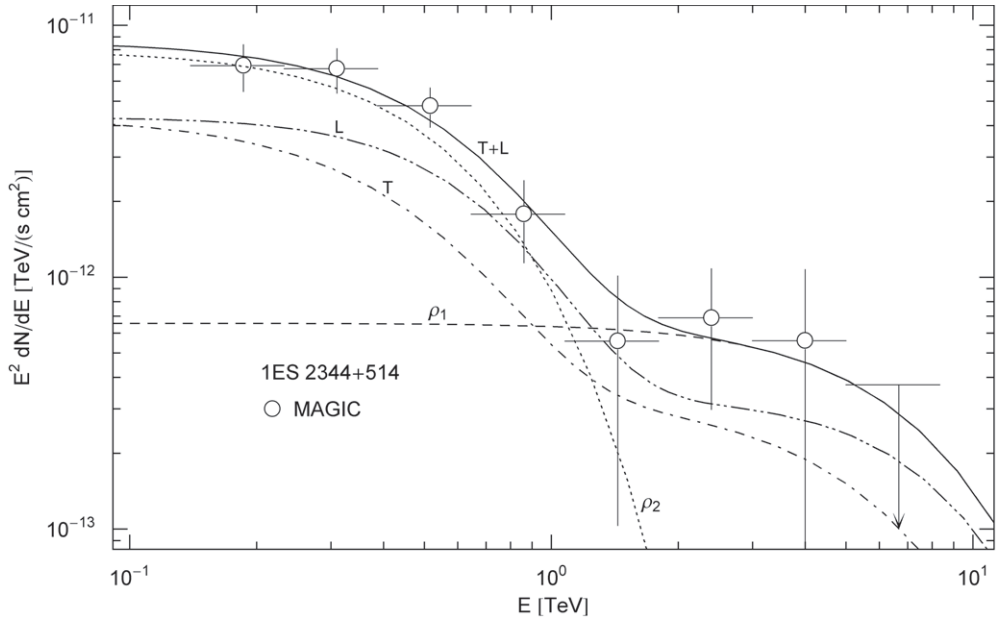

Fig. 3: Spectral map of the TeV blazar 1ES 2344 + 514. MAGIC data points from ref. [3], notation as in figs. 1 and 2. The cutoff energy is 2.8 TeV for the ρ_1 cascade and 220 GeV for ρ_2. The spectral curvature of the rescaled flux density $E^2 \mathrm{d}N^{\mathrm{T+L}}/\mathrm{d}E$ is generated by the Boltzmann factor of the thermal electron populations, cf. (3) and table 1.

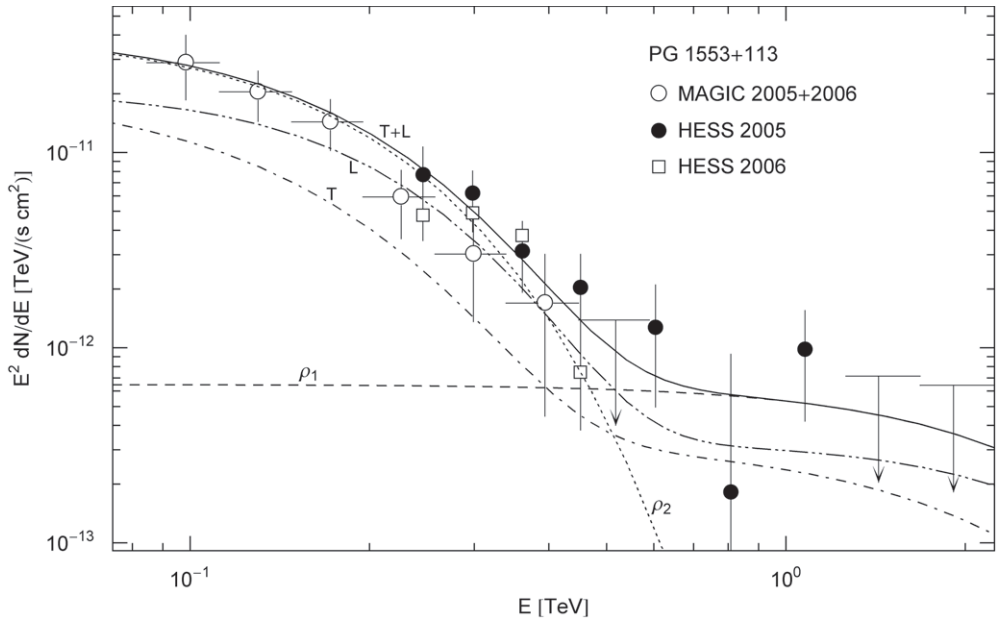

Fig. 4: Spectral map of the BL Lac object PG 1553 + 113. MAGIC flux points from ref. [14], HESS points from ref. [15]. The plots are labeled as in fig. 1. The ρ_2 cascade is cut at 65 GeV, the cutoff of the high-energy cascade ρ_1 is at about 1 TeV. The spectral curvature is comparable to that of the BL Lac 1ES 2344 + 514 in fig. 3, despite the higher redshift of PG 1553 + 113, cf. table 1, suggesting that the curvature of the plotted flux density is intrinsic rather than due to intergalactic absorption.

This expansion is valid for $\beta = m/kT \ll 1$, and the second term in the parentheses has to be small compared to 1. We may combine these two conditions as $T_{\mathrm{F}}/T \ll 1$, where $kT_{\mathrm{F}} = \sqrt{p_{\mathrm{F}}^2 + m^2}$ is the relativistic Fermi energy with $p_{\mathrm{F}} = (3\pi^2 n^{\mathrm{e}}/V)^{1/3}$. Equation (9) is derived from the high-temperature fugacity expansion of a Fermi distribution, of which the classical density (3) is the leading order, cf. *e.g.* ref. [13].

The tachyonic spectral fit of blazar 1ES 2344 + 514 ($z \approx 0.044$) [3] is depicted in fig. 3, and that of blazar PG 1553 + 113 [14,15] in fig. 4. The flux points were collected with the air Cherenkov detectors MAGIC and

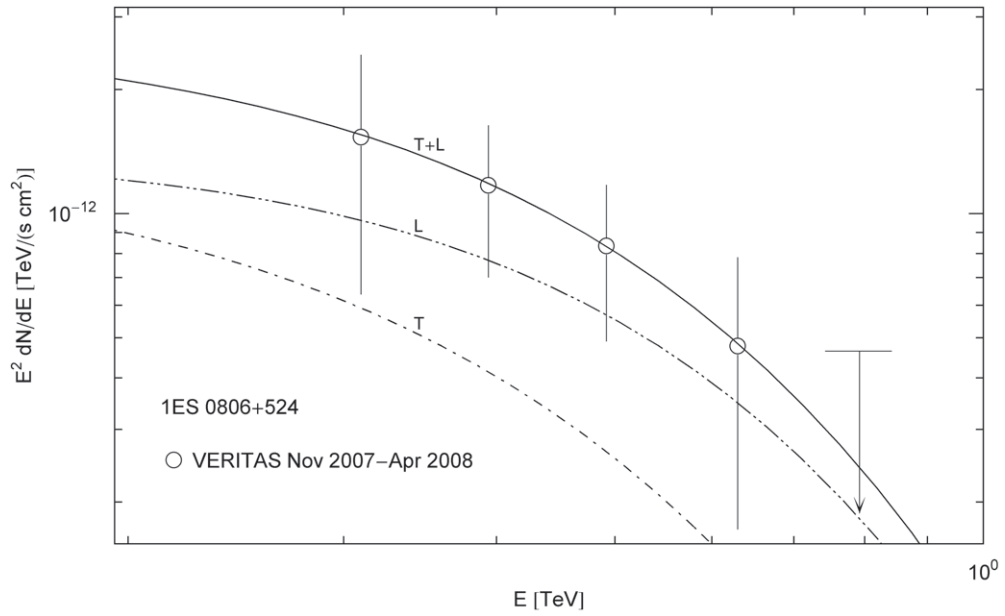

Fig. 5: Spectral map of the BL Lac object 1ES $0806+524$. VERITAS flux points from ref. [5]. There is only one cascade $\mathrm{T}+\mathrm{L}=\rho_1$ in the depicted 0.2–1 TeV interval. The spectral cutoff occurs at 160 GeV. One may compare the spectral slope to the high-energy slope of quasar 3C 279 in fig. 2 of ref. [19], whose redshift is almost four times that of 1ES $0806+524$, although the spectral curvature is quite similar. Conversely, the BL Lac H1426 + 428 has a similar redshift, but its spectral curvature is less pronounced, cf. fig. 3 of ref. [6]. The spectral curvature is thus uncorrelated with redshift.

HESS. The redshift of PG $1553+113$ is still unclear due to its featureless spectrum; the estimate of $z\approx 0.36$ is based on a contested absorption line [4], a lower bound of $z>0.09$ is given in ref. [16]. The spectral map is not affected by the distance estimate, but the source number and internal energy of the electron populations are. We therefore list these quantities in table 1 for $z\approx 0.1$ as well as $z\approx 0.36$. The cascade fit of the BL Lac 1ES $0806+524$ at $z\approx 0.138$ [17] is shown in fig. 5.

High-energy spectral slopes of Galactic TeV γ-ray sources and active galactic nuclei: a comparative study. – High-energy γ-ray spectra of active galactic nuclei (AGNs) are usually assumed to be generated by inverse Compton scattering or *pp* scattering followed by π^0 decay [9,14]. Both mechanisms result in a flux of high-energy photons partially absorbed by interaction with the infrared background radiation. By contrast, there is no absorption of tachyonic γ-rays, since tachyons cannot directly interact with photons. We may compare figs. 2–5 to the spectral maps of the AGNs H1426 + 428 ($z\approx 0.129$, 570 Mpc) and 1ES $1959+650$ ($z\approx 0.047$, 210 Mpc) in ref. [6], 1ES $0229+200$ ($z\approx 0.140$, 620 Mpc) in ref. [18], and the radio quasar 3C 279 ($z\approx 0.538$, 2.4 Gpc) in ref. [19]. The curvature of these spectra is uncorrelated with distance. For instance, there is no increase of the spectral curvature with redshift that could indicate absorption, when comparing the blazar 1ES $0347-121$ ($z\approx 0.188$, 830 Mpc) in fig. 2 of ref. [18] to the BL Lac 1ES $2344+514$ ($z\approx 0.044$, 190 Mpc) in fig. 3. The nearer source has even steeper spectral slopes.

Moreover, the spectral maps of some Galactic TeV sources look quite similar to those of AGNs, which likewise indicates unattenuated intergalactic propagation of TeV γ-rays. The spectral maps of the Markarian galaxies Mkn 501 (at 150 Mpc) and Mkn 421 (140 Mpc) in figs. 5 and 6 of ref. [6] are to be compared to the Galactic TeV sources HESS $J1303-631$ in fig. 3 and HESS $J1825-137$ in fig. 5 of ref. [7], as well as to the microquasar LS 5039 in fig. 2 of ref. [12]. The curved spectral slopes of the Galactic sources are steeper than of the AGNs. Therefore, absorption of electromagnetic radiation due to interaction with background photons is not a viable explanation of spectral curvature, since the curvature would increase with distance if affected by intergalactic absorption. In fact, photonic attenuation theories have constantly overestimated the attenuation, owing to intricate modeling with vaguely known cosmological input parameters, which come on top of the fitting parameters of the inverse-Compton or hadronic radiation models. An electromagnetic spectral fit of BL Lac 1ES $2344+514$ is depicted in fig. 6 of ref. [3], which can be compared to the tachyonic counterpart in fig. 3.

The common feature in the γ-ray wideband of TeV blazars is the extended MeV-to-GeV spectral plateau, cf. fig. 1. The low-energy cascades in figs. 3–5 also extend further into the GeV band as spectral plateaus, but only the decaying slopes are depicted, owing to the lack of data points in the lower GeV range to compare with. One may thus predict Fermi blazars to exhibit a spectral plateau in the E^2-rescaled flux representation used in the figures, since Fermi flux points are unlikely to significantly

differ from EGRET observations, apart from the error bars. In the high GeV region, the plateaus will bend into exponential decay, notably without a power law transition, cf. the discussion below. In brief, the spectral maps of Fermi blazars combined with Cherenkov observations will be structured like the γ-ray broadband of W Com in fig. 1.

Conclusion. – Tachyonic γ-ray spectra of TeV blazars are generated by thermal ultra-relativistic electron populations in the galactic nuclei. Tachyons are radiation modes, unrelated to electromagnetic radiation. The tachyon mass refers to the radiation field rather than the current [20], in contrast to the traditional approach based on a current of superluminal source particles emitting electromagnetic radiation [21–25]. The tachyonic radiation modes are coupled by minimal substitution to the electron current. The negative mass-square of tachyons implies superluminal velocity and allows longitudinal polarization [19]. The tachyonic radiation field does not couple to electromagnetic fields, nor is it affected by electric charge. Interaction of tachyons with photons can only happen indirectly via matter fields. Thus, in contrast to electromagnetic γ-rays, there is no extinction of the extragalactic tachyon flux by the cosmic background light.

The cascade spectra in figs. 1–5 are produced by the tachyonic radiation density averaged over the electron populations of the AGNs, cf. (6). The radiation density (1) is generated by electrons in uniform motion [26]; there is no radiation damping, as photons can only be radiated by accelerated charges, in contrast to tachyonic quanta, where the emission rate primarily depends on the electronic Lorentz factor rather than on acceleration [27,28]. Superluminal synchrotron radiation from ultra-relativistic electrons orbiting in magnetic fields was investigated in ref. [29]. In the zero-magnetic-field limit, the averaged tachyonic synchrotron densities converge to the densities (1). The orbital curvature induces modulations in the high-energy slope of these densities, but the ripples are smoothed out when performing a pitch-angle average, cf. figs. 1–3 of ref. [29]. Thus we can use uniform radiation densities even in the presence of magnetic fields in the galactic nuclei. In this case, if the trajectories are bent by magnetic fields, there are radiation losses due to the electromagnetic curvature radiation. In the absence of sizeable magnetic fields and other scattering mechanisms, high Lorentz factors and temperatures are sustainable owing to the lack of radiation damping, the superluminal radiation being generated by inertial electrons. The high plasma temperature inferred from the spectral fits, cf. table 1, implies ultra-high energy electrons in the AGNs. Such high electron temperatures are also found in Galactic pulsar wind nebulae, possible production sites of ultra-high–energy cosmic rays [7,30,31].

The γ-ray cascades of TeV blazars are radiated by thermal electron populations depending on two fitting parameters, the electron number and temperature [6,32]. By contrast, the shock-heated electron plasma of supernova remnants requires a nonthermal fit with the electron index δ as third parameter, so that the density (3) is replaced by $\mathrm{d}\rho \propto \mathrm{e}^{-\beta\gamma}\sqrt{\gamma^2-1}\gamma^{1-\delta}\mathrm{d}\gamma$ in the Boltzmann average (6). A non-zero δ can result in a power law slope joining the spectral plateau to the curved exponentially decaying slope, cf. the spectral maps of the supernova remnants W28 in fig. 4 of ref. [18] and RX J1713.7 − 3946 in fig. 2 of ref. [6] as well as the cascade fits of the Galactic TeV sources in refs. [31,33]. Here, we have demonstrated that the thermal ($\delta = 0$) γ-ray cascades of BL Lac objects are exponentially cut without power-law crossover, and that the exponential decay manifested in the curved spectral slopes in figs. 1–5 is solely caused by the Boltzmann factor of the electron densities, as tachyonic γ-rays propagate unattenuated over intergalactic distances.

REFERENCES

[1] Tagliaferri C. *et al.*, *Astron. Astrophys.*, **354** (2000) 431.
[2] Scalzo R. A. *et al.*, *Astrophys. J.*, **607** (2004) 778.
[3] Albert J. *et al.*, *Astrophys. J.*, **662** (2007) 892.
[4] Osterman M. A. *et al.*, *Astron. J.*, **132** (2006) 873.
[5] Acciari V. A. *et al.*, *Astrophys. J.*, **690** (2009) L126.
[6] Tomaschitz R., *Eur. Phys. J. C*, **49** (2007) 815.
[7] Tomaschitz R., *Ann. Phys. (N.Y.)*, **322** (2007) 677.
[8] Tomaschitz R., *Eur. Phys. J. B*, **17** (2000) 523.
[9] Acciari V. A. *et al.*, *Astrophys. J.*, **684** (2008) L73.
[10] Hartman R. C. *et al.*, *Astrophys. J. Suppl.*, **123** (1999) 79.
[11] Böttcher M., Mukherjee R. and Reimer A., *Astrophys. J.*, **581** (2002) 143.
[12] Tomaschitz R., *Physica A*, **385** (2007) 558.
[13] Tomaschitz R., *Physica A*, **387** (2008) 3480.
[14] Albert J. *et al.*, *Astrophys. J.*, **654** (2007) L119.
[15] Aharonian F. *et al.*, *Astron. Astrophys.*, **477** (2008) 481.
[16] Sbarufatti B. *et al.*, *Astron. J.*, **132** (2006) 1.
[17] Nilsson K. *et al.*, *Astron. Astrophys.*, **475** (2007) 199.
[18] Tomaschitz R., *Phys. Lett. A*, **372** (2008) 4344.
[19] Tomaschitz R., *EPL*, **84** (2008) 19001.
[20] Tomaschitz R., *Eur. Phys. J. D*, **32** (2005) 241.
[21] Sommerfeld A., *Proc. K. Akad. Wet. Amsterdam, Sect. Sci.*, **7** (1904) 346.
[22] Tanaka S., *Prog. Theor. Phys.*, **24** (1960) 171.
[23] Terletsky Ya. P., *Sov. Phys. Dokl.*, **5** (1961) 782.
[24] Feinberg G., *Phys. Rev.*, **159** (1967) 1089.
[25] Newton R., *Science*, **167** (1970) 1569.
[26] Tomaschitz R., *Physica A*, **320** (2003) 329.
[27] Wheeler J. A. and Feynman R. P., *Rev. Mod. Phys.*, **17** (1945) 157.
[28] Tomaschitz R., *Class. Quantum Grav.*, **18** (2001) 4395.
[29] Tomaschitz R., *Phys. Lett. A*, **366** (2007) 289.
[30] Nagano M. and Watson A. A., *Rev. Mod. Phys.*, **72** (2000) 689.
[31] Tomaschitz R., to be published in *Physica B* (2008) doi: 10.1016/j.physb.2008.12.026.
[32] Tomaschitz R., to be published in *Opt. Commun.* (2009) doi: 10.1016/j.optcom.2009.01.024.
[33] Tomaschitz R., *Astropart. Phys.*, **27** (2007) 92.